Int. J. Microgravity Sci. Appl. Vol. 30 No. 1 2013 (11–18)

Theorization and Modeling Ⅲ
(Review)

Crystal Nucleation in Supercooled Liquid Metals

Kenneth F. Kelton

Abstract

It is becoming increasingly clear that nucleation processes in liquids and glasses are more complicated than previously thought, often coupling to other phase transitions and ordering processes. Experimental and theoretical studies show the development of icosahedral short-range order in many supercooled transition metal and alloy liquids, which in some cases extends beyond nearest neighbor distances. This atomic and chemical ordering couples to the nucleation barrier, and may play a role in glass formation in some cases. Select experimental results are presented to demonstrate these points. These are discussed in light of nucleation theories, including the commonly used Classical Theory of Nucleation, diffuse interface theories, and coupled-flux theory, which takes account of the interaction between interfacial processes at the surface of the crystal nuclei and long-range diffusion fluxes.

Keyword(s): nucleation, supercooling, liquid structure, glass formation

1. Introduction

Phase transitions are ubiquitous, ranging from the solidification of liquids, to solid-state transformations, to the precipitation of kidney stones, and even to changes in the early universe. Most of these phase transitions are initiated by a *nucleation* step. In this step large changes in some order parameter, which characterizes the difference between the initial and transformed phases, occurs within spatially small regions. Liquid solidification is often used for the investigation of nucleation processes because strain effects, which complicate nucleation studies in solids, are effectively absent. Under the right conditions liquids can be maintained for long periods of time at temperatures below their equilibrium melting (or liquidus) temperatures, i.e. in a *supercooled* state. That this is possible indicates the existence of a barrier to the formation of the stable crystal phases, generally called the *nucleation barrier*.

As will be shown in this article, even in metallic liquids nucleation is complicated, challenging current understanding. The thermodynamic model that underlies the most commonly used model for nucleation, the Classical Theory of Nucleation, is questionable when applied to the small clusters involved in the nucleation step. Inherent chemical and topological ordering in the volume of the liquid, and ordering near the interface with the growing crystal and near surfaces, are not fully included in nucleation theories, although some progress been has made using density functional approaches. The nucleating phase often has a chemical composition that is different from that of the parent phase, making long-range diffusion effects potentially important. To treat this problem correctly, the stochastic interfacial processes described by most nucleation theories must be coupled with the stochastic diffusion field, which is only rarely done. Finally, there is a great deal of interest in metallic glass formation, which requires that crystallization be effectively bypassed. An understanding of the kinetics of crystal nucleation during rapid cooling and how nucleation depends on the structural evolution of the liquid is needed to treat this problem. These points are briefly surveyed in this article.

2. Nucleation Theory

Before looking at experimental data, it is useful to discuss briefly the current state of nucleation theory.

2.1 Classical Theory of Nucleation

In *homogenous nucleation*, small regions of crystalline order arise spontaneously by spatially and temporally independent fluctuations within the supercool liquid. In *heterogeneous nucleation* these fluctuations are catalyzed at specific sites. Both types of nucleation are most often analyzed within the Classical Theory of Nucleation (CNT).[1] In homogeneous CNT, small regions of the crystal phase (clusters) develop randomly in space and time by a series of kinetic reactions in which single atoms or molecules (monomers) attach and detach from the cluster interface. Assuming spherical clusters, negligible strain, and a sharp interface between the crystal and amorphous phase, the reversible work of formation of a cluster of n monomers is:

$$W_n = n\Delta\mu + (36\pi)^{1/3}\,\bar{v}^{2/3}\,n^{2/3}\,\sigma \qquad (1)$$

Here $\Delta\mu$ is the Gibbs free energy of the crystal phase less than that of the glass phase per monomer, $\bar{v}$ is the monomer volume, and σ is the liquid-crystal interfacial free energy per unit surface area. The competition between the volume free energy favoring cluster formation and the surface free energy opposing it leads to a maximum in the work of formation, W_{n^*}, for a critical cluster size, n^*. Clusters are assumed to evolve slowly by a series of bimolecular reactions, where the rate of change of the

Department of Physics, Campus Box 1105, Washington University, One Brookings Drive, St. Louis, Missouri 63130 USA
(E-mail: kfk@wustl.edu)

time-dependent population density as a function of the cluster size, n, and time, t, is

$$\frac{dN_{n,t}}{dt} = N_{n-1,t}\,k^{+}_{n-1} - N_{n,t}\left[k^{+}_{n} + k^{-}_{n}\right] + N_{n+1,t}\,k^{-}_{n+1} \quad , \qquad (2)$$

where k^{+}_{n} is the rate of monomer addition to a cluster of size n and k^{-}_{n} is the rate of monomer loss. Assuming interface-limited kinetics (strictly valid only for nucleation processes where the initial and final phases have the same chemical composition) $k^{\pm}_{n} = 4n^{2/3}\gamma^{\pm}_{n}$. For spherical clusters, the first term ($4n^{2/3}$) is the number of attachment sites on the surface of the cluster, and, $\gamma^{\pm}_{n} = \frac{6D}{\lambda^2}\exp\left(\mp\frac{\delta W_n}{2k_{\mathrm{B}}T}\right)$ where D is the diffusion coefficient in the liquid, λ is the jump distance, k_{B} is Boltzmann's constant, T is the temperature and $\delta W_n = W_{n+1} - W_n$. The nucleation frequency, $I_{\mathrm{n,t}}$, is the time- and size-dependent flux from clusters of size n to ones of size n+1 ($I_{n,t} = k^{+}_{n}N_{n,t} - k^{-}_{n+1}N_{n+1,t}$). Except for extremely rapid cooling rates (see Section 3.3), time-dependent effects are generally not important for crystallization from the liquid, although they can play a very prominent role in glass crystallization[2),3)].

To a lowest approximation, the nucleation rate is the forward flux of clusters past the critical size. To obtain a more quantitative expression, assuming a time-invariant (steady-state) cluster distribution ($N_{n,t} \to N^{st}_{n}$), the steady-state nucleation rate is

$$I^{st} = \frac{24D\,(n^{*})^{2/3}N_A}{\lambda^2}\left(\frac{|\Delta\mu|}{6\pi k_B T n^{*}}\right)^{1/2}\exp\left(-\frac{W_{n^*}}{k_B T}\right), \qquad (3)$$

where the critical size, n^{*}, is $32\pi\sigma^3/3\,\bar{v}\,|\Delta g|^3$, the critical work of formation, W_{n^*} (called the *nucleation barrier*) is $16\pi\sigma^3/3\bar{v}\,|\Delta g|^2$ (where $\Delta g = \Delta\mu/\bar{v}$), and N_{A} is the total number of monomers in the system, typically taken to be Avogadro's number per mole (see Ref. 1 for more details). Frequently, solid impurity sites, such as a container wall, lower the value of W_{n^*}, which from Eq. (3) will increase the nucleation rate. Within CNT, this is taken into account by multiplying W_{n^*} by a factor $f(\theta)$ that varies between 0 and 1 depending on the contact angle, θ, between the crystal phase and the solid (see Ref. 1 for a detailed discussion of heterogeneous nucleation).

Equation (3) predicts a sharp increase in the nucleation rate with decreasing temperature due to the increasing driving free energy, followed by a decrease at lower temperatures due to the slowing atomic dynamics. This predicted behavior is in good agreement with experimental data[1),4)]. A fundamental problem with CNT is that the magnitude of the nucleation rate is extremely sensitive to the value of the interfacial energy, which is generally only known from fits to nucleation data.

2.2 Diffuse Interface Theories

The CNT assumes that the interface between the volume and surface contributions to the work of cluster formation can be cleanly divided (Eq. (1)), requiring a sharp interface between the nucleating cluster and the parent liquid phase. However, this interface is actually diffuse [5)-7)], with a width that is of the order of the radius of the nucleation clusters when the driving free energy is large. The regions of the liquid near the cluster are, therefore, more ordered than expected within CNT.

A phenomenological model to account for the ordering was proposed independently by Gránásy[8)-10)] and Spaepen[11)]. Ordering in the liquid ahead of the advancing cluster interface implies that the Gibbs free energy $g(r)$ will change continuously on crossing the cluster boundary. To lowest order, this can be described by the step-function shown in **Fig. 1**, allowing the work of cluster formation to be readily obtained,

$$W_{n^*} = \frac{4\pi}{3}\Delta g_{il}\,\delta^3\frac{b^2}{(1-b)^2} \qquad (4)$$

where δ is the interfacial width, $b^2 = 1 - (\Delta g_{sl}/\Delta g_{il})$, Δg_{sl} is the free energy difference of the liquid and solid phases ($g_s - g_l$), and Δg_{il} is the free energy difference between the liquid and interface ($g_i - g_l$). By Equating this value for W_{n^*} with that obtained from the CNT, an expression for the interfacial free energy is obtained, $\sigma_{ls} \approx \delta(\Delta g_{il} - \Delta g_{sl}/2)$. A key result from this model is that σ_{ls} is predicted to have a positive temperature dependence in agreement with experiment [12)]. Here, a simplistic profile was considered. The precise profile of $g(r)$ can be obtained from a density-functional theory (DFT) approach in terms of one or more order parameters that characterize the initial and transformed phases.

In principle a DFT formalism can also be used to account for coupling of nucleation processes to other phase transitions in the parent phase (such as chemical or magnetic ordering transitions). For illustration, consider the semi-empirical density functional

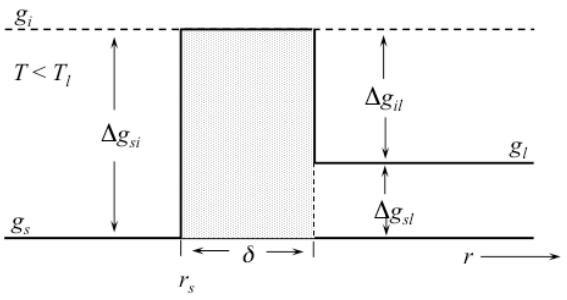

Fig. 1 Step-function change of the free-energy density through the interfacial region between the liquid and solid (from r_s to $r_s+\delta$. (Adapted from Ref. 11, copyright (1994), with permission from Elsevier.)

approximation (SDFA), where a single order parameter, M, is assumed. In the liquid far from the cluster, $M(r,t)$ is zero; it is equal to one for an infinitely large solid cluster. The free energy can be written as a functional of M, $G\left[M\left(r,t\right)\right]$, and the work of cluster formation can be computed in a similar way as from the CNT, $W[M]=\int_V \left(g(M(r,t)) - \mu(M(r,t))\right) dr$ (see Refs. 1 and 13) for a detailed treatment). **Figure 2** shows the computed order parameter, M, as a function of distance from the center of the cluster for three different values of $\tilde{\Delta}$, which is a scaled parameter that corresponds to the driving free energy. The values for $\tilde{r}_s^*$, the corresponding scaled critical radii, are listed in the figure. Like the CNT, increased magnitudes of the driving free energy give smaller values for the critical size. However, for all values of $\tilde{\Delta}$ the interface is diffuse. As shown in the inset, only when $\tilde{\Delta}$ becomes very small (= -0.05, corresponding to $\tilde{r}_s^*=20$) does the interface approach the sharp boundary assumed in CNT. Further, although M should be unity in the solid phase, it does not reach that value even in the center of the cluster, except when the driving free energy is very small. Calculations also show that the CNT overestimates the work of cluster formation for larger driving free energies. Taken together, these results indicate that the CNT is only quantitatively correct when the departure from equilibrium is small, i.e. near the melting (or liquidus) temperature. Although not discussed here, studies show that the DIT and SDFA models fit nucleation rate data in liquids and glasses better than the CNT, demonstrating the importance of the ordering in the liquid near the cluster interface[1), 14)].

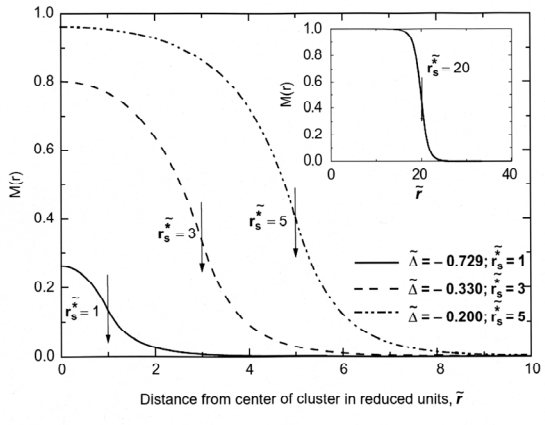

Fig. 2 Order parameter M as a function of the scaled distance from the center of the critical cluster. Profiles are shown for three different values of the scaled driving free energy, $\left|\tilde{\Delta}\right|$. (Reprinted from Ref. 13, copyright (1994), American Institute of Physics.)

2.3 Coupled Flux Theory - Incorporation of Long-Range Diffusion

The nucleation theories previously discussed are interface-limited theories, appropriate if the chemical composition of the nucleating phase is the same as that of the liquid (polymorphic crystallization), or if the diffusion rates in the liquid are much faster than the interfacial attachment kinetics. The latter can make CNT particularly inappropriate for solid-state precipitation [15),16)], but it is generally not an important issue for nucleation from the liquid if the temperature is constant or slowly varying. When the interfacial attachment rates to the cluster do become competitive with the diffusive transport rates in the liquid, these two stochastic fluxes become coupled.

Following an approach first suggested by Russell [18)], this may be treated to lowest order by focusing attention on three regions **(Fig. 3)**: the cluster, the immediate neighborhood around the cluster (the shell region), and the parent phase [17),19)]. In this *Coupled*-Flux Model (CFM), the flux between the shell and the parent phase is coupled with that between the shell and the cluster. The cluster evolution underlying time-dependent nucleation is determined by solving numerically a system of coupled differential rate equations that incorporate the interfacial and shell/parent phase fluxes. Numerical solutions show that the coupled-fluxes can significantly lower the nucleation rate and increase the induction time for nucleation beyond the predictions from the CNT. Surprisingly, a key prediction of CFM is that for sub-critical clusters, the liquid composition is closer to that of the precipitating cluster, in contradiction with expectations based on the growth of large clusters. These predictions have been confirmed in Kinetic Monte Carlo simulations that probe the growth and shrinkage of clusters in a simple lattice gas model, augmented with adjustable diffusion kinetics [20)].

While coupling of the interfacial and diffusive fluxes typically has little influence on nucleation from supercooled

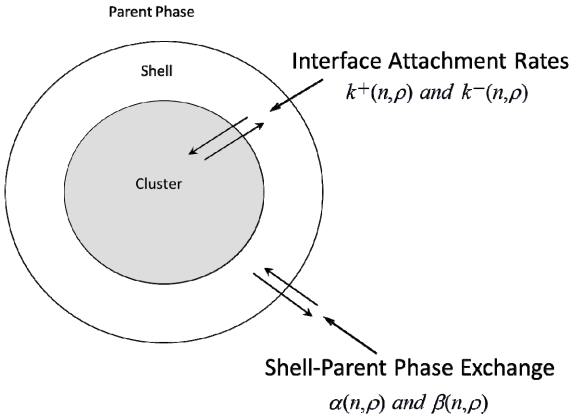

Fig. 3 A schematic illustration of the fluxes in the Coupled-Flux Model. (Reprinted from Ref. 17, copyright (2000) with permission from Elsevier.)

liquids, it can have a significant effect for nucleation during a rapid quench (see Section 3.3) and in glass devitrification [21]. Coupled-flux effects may also be important for nucleation under quiescent micro-gravity conditions, where stirring (which is always present in a terrestrial environment) is suppressed.

3. Nucleation Studies in Metallic Liquids

3.1 Experimental Techniques

Heterogeneous nucleation, on impurities in the liquid or on the container walls, generally dominates the solidification of liquid metals. Since the number of heterogeneous sites and their catalytic efficiencies are generally unknown, a quantitative analysis of such nucleation data is difficult or impossible. For this reason, techniques have been developed to minimize the impact of heterogeneous nucleation, so that homogeneous nucleation may be studied (see Refs. 1 and 4 for a more extended discussion than provided here). These include (i) *isolation*, where impurities are compartmentalized into a small volume fraction of the liquid[12),22),23)], (ii) *fluxing*, where the liquid is coated with a material that dissolves or renders ineffective impurities and protects it from the container walls and (iii) *containerless processing*, where liquids are held without containers in vacuum or a high-purity non-oxidizing atmosphere. The most common containerless techniques are based on aerodynamic levitation, electromagnetic levitation (EML) and electrostatic levitation (ESL) [1),24)]. Aerodynamic levitation is achieved by a controlled gas flow through nozzles of optimal design for the size and density of the samples of interest. However, the flowing gas makes temperature and positioning control difficult, may lead to heterogeneous nucleation on gas impurities, and cannot be used for quantitative measurements of thermophysical properties. EML uses a high frequency EM field to induce eddy currents in metallic samples, providing levitation from Lenz's law. However, since both heating and levitation are coupled in EML[24)], it is not always possible to supercool the liquid while maintaining sample levitation under terrestrial conditions. Further, only metallic materials, or semiconducting materials that become metallic in the liquid phase (e.g. Si), can be studied. Electrostatic levitation (ESL) is the most versatile, offering several key advantages over aerodynamic and electromagnetic levitation: (1) non-metallic as well as metallic systems can be studied; (2) the heating and positioning power are decoupled, allowing measurements in more deeply supercooled liquids; and (3) the rf coils required for electromagnetic levitation limits the view of the sample while ESL provides a wide range of access to the sample. In ESL charged samples with a 2.0 – 3.0 mm diameter (approximately 30-70 mg mass) are levitated by Coulomb forces in an electrostatic field (0 to 2 MV/m) under high vacuum (typically 10^{-7} – 10^{-8} torr) [25), 26)]. The samples are initially charged by induction. During processing the charge is maintained with an external UV source at low temperatures and by thermionic emission at high temperatures. Three pairs of orthogonal electrodes and a robust control algorithm[27),28)] maintain the sample position during processing to within 50-100 μm, based on error signals from two orthogonal position-sensitive detectors, which are provided as input to the DC amplifiers connected to the electrodes. The sample can then be heated to any temperature up to ≥ 3000 K using one or more lasers. Our liquid diffraction data, some discussed in this review, were obtained using an ESL facility (WU-Beamline ESL, or WU-BESL) (**Fig. 4**) that has been constructed at Washington University and optimized for X-ray diffraction studies of the levitated supercooled liquids [29)]. A schematic of the transmission X-ray diffraction geometry is shown in **Fig. 4.c**. Complementary physical property data, such as maximum supercooling, density, surface tension and viscosity, can be obtained in ESL, allowing the liquid structure to be linked with the crystal nucleation barrier (Section 4) and with thermophysical properties.

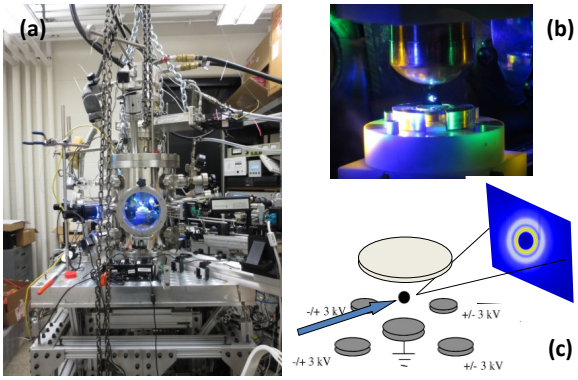

Fig. 4 (a) Photograph of the ESL at Washington University, optimized for X-ray scattering studies. (b) A levitated sphere; the different colors of light are from the high-intensity LEDs used in the sample positioning feedback algorithm. (c) Schematic diagram showing the incoming and scattered X-rays in a transmission geometry from a levitated liquid sample; the diffraction pattern is recorded on an area detector. The vertical and two sets of side electrodes used for levitation and positioning are also shown (*c* is courtesy of N. A. Mauro).

3.2 Maximum Undercooling Results for Elemental Liquids

Since, as demonstrated in studies of nucleation in silicate glasses, the steady-state nucleation rate rises rapidly with supercooling [4)], and the growth velocities in the supercooled liquid are large, the time scale for crystallization is dominated by the time required to form a nuclei. Experimental studies show that the *reduced undercooling* ($\Delta T_r = (T_m - T_u)/T_m$, where T_m is the melting temperature and T_u is the minimum

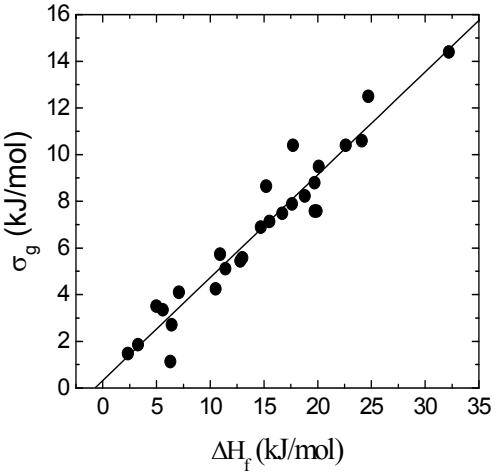

Fig. 5 Interfacial free energy obtained from maximum supercooling studies of elemental metallic liquids, shown as a function of the heat of fusion. (Reprinted from Ref. 4, copyright (1991), with permission from Elsevier.)

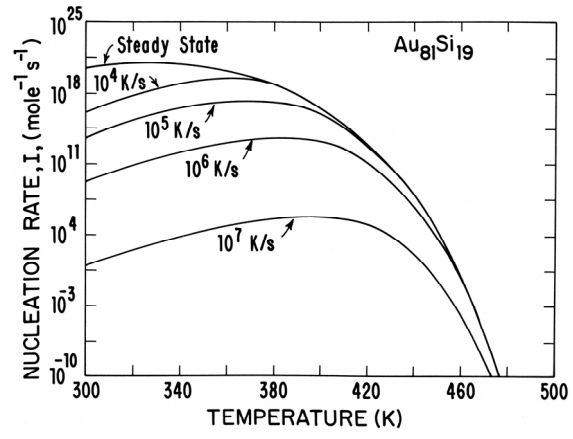

Fig. 6 Calculated homogeneous nucleation rate for $Au_{81}Si_{19}$ as a function of temperature and quenching rate. (Reprinted from Ref. 31, copyright (1986), with permission from Elsevier.)

temperature to which the liquid can be cooled before crystallizing) for pure liquid metals is in the range 0.1 to 0.4. This indicates that the barrier to nucleation is large. An analysis of compiled data (see Refs. 1 and 4) demonstrates that the *gram-atomic* interfacial free energy ($\sigma_{ls}^{M} = \sigma_{ls} V^{2/3} N_A^{2/3}$, where σ_{ls} is the interfacial free energy determined from fits to Eq. (3), V is the molar volume and N_A is Avogadro's number), scales linearly with the heat of fusion ($\sigma_{ls}^{M} \approx 0.44\ \Delta h_f$) (**Fig. 5**), suggesting a "bond-breaking-like" process to form the interface.

3.3 Nucleation and Glass Formation

Much of the current interest in the study of metallic liquids is to gain a better understanding of glass formation. Ultimately, this is a question of nucleation and growth, since if significant crystallization can be avoided the liquid will transform to a glass at the glass transition temperature. Traditional silicate glasses are formed at modest cooling rates, of order 1 K/s or less. Until recently, much higher cooling rates, 10^5 – 10^{12} K/s, were required to form metallic glasses. Now there are many alloys in which glasses can be formed with cooling rates that are more typical of silicate glasses.

The expected number of nuclei that form during the quench is

$$N = \int_0^t I\,dt \rightarrow R^{-1} \int_{T_1}^{T_2} I(T)\,dT \ , \qquad (5)$$

where R is the quenching rate, and T_1 and T_2 are the upper and lower end of the temperature range over which nucleation is significant. Assuming steady-state nucleation and using parameters obtained from crystallization studies of $Au_{81}Si_{19}$, one of the first known metallic glasses, approximately 10^{16}-10^{18} quenched-in nuclei/mol are predicted from Eq. (5) with a quenching rate of 10^6 K/s. While some number of quenched-in nuclei is unavoidable, the large number predicted for $Au_{81}Si_{18}$, when coupled with reasonable estimates of the growth velocity would predict that at least 1% of the quenched sample would be crystallized. No evidence of crystallization is observed, however. Greer first showed experimentally that the number of quenched-in Fe-B glasses scaled as $R^{-2\ to\ 4}$, not to R^{-1} as predicted from Eq. (5) [30]. A likely reason for this is that the assumption of a steady-state nucleation rate during cooling is incorrect. During a rapid quench there is insufficient time to maintain the steady-state distribution that is appropriate for each temperature. This is why transient nucleation effects are observed in glass crystallization experiments; the cluster size distribution obtained at the end of the quench is not the appropriate one at the annealing temperature, but is more similar to the steady-state distribution at a higher temperature. Numerical studies have shown that the nucleation rate during the quench can be significantly lower than the expected steady-state rate (**Fig. 6**), making glass formation easier and increasing the stability of the glass to crystallization [31]. This becomes particularly important if, as is usually the case, the chemical compositions of the crystal phases that can form during the quenching are different from that of the liquid, since the transient times become much longer than for the case of polymorphic crystallization [17), 32].

4. Developing Structure in Supercooled Liquids – Impact on Phase Transitions

From the discussion in Section 2.2, experimental and theoretical evidence indicate that the liquid is ordered close to the interface of the nucleating cluster. But does order inherently develop

within a supercooled liquid, independent of the presence of crystal nuclei? And does this order influence liquid crystallization? In 1952, Charles Frank proposed that the answer to both questions was *yes* [33]. To explain the ability to significantly supercool liquid metals, first demonstrated by Turnbull, Frank proposed that metallic liquids contain a large amount of icosahedral short-range order (ISRO). Because the point-group symmetry of the icosahedron is incompatible with translational periodicity, Frank argued that this low energy structure in the liquid was the source of the barrier to the nucleation of the crystal phase, allowing the liquid to be deeply supercooled.

Many MD simulations are consistent with Frank's hypothesis. One example of the results of an ab-initio MD simulation for binary and ternary Cu-Zr based glass-forming liquids is shown in **Fig. 7**. A dramatic increase in the number of <0,0,12,0> Voronoi polyhedron (reflecting ISRO) is observed between the liquidus temperature, T_l, and the glass transition temperature, T_g. This is consistent with experimental results in a $Zr_{59}Ti_3Cu_{20}Ni_8Al_{10}$ glass-forming liquid [3].

4.1 Measurements of Short-Range Order in Liquids and Glasses

Nucleation measurements provided the first experimental evidence for icosahedral order in amorphous metals, with a very small interfacial free energy (σ_{il}) measured between a metallic glass and the primary crystallizing icosahedral quasicrystal (i-phase) [35]. This was subsequently confirmed by quantitative time-dependent nucleation measurements of i-phase formation in a $Zr_{59}Ti_3Cu_{20}Ni_8Al_{10}$ metallic glass, obtaining σ_{il} = 0.01 ± 0.004 Jm^{-2}, much smaller than expected for a crystal phase.
Holland-Moritz and co-workers made the first systematic study of the supercooling of liquids. They found that as the icosahedral short-range order in the crystallizing phases

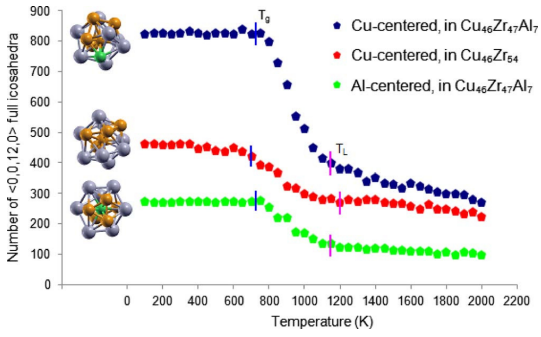

Fig. 7 The results of ab-inito MD calculations showing the growth of the number of <0,0,12,0> Voronoi polyhedral as a function of supercooling in Cu-Zr based liquid alloys. (Reprinted with permission from Ref. 34), copyright (2008), American Institute of Physics.)

increased, the interfacial free energy decreased, as expected from the previous glass studies [36), 37)].

Over the past ten years there has appeared direct structural evidence for ISRO from X-ray and neutron diffraction studies of supercooled liquids, using electromagnetic and electrostatic levitation scattering techniques. The structure factor, S(q), is easily obtained directly from the scattering data. The pair-distribution function, g(r), which give the angular-averaged radial probability distribution of atom locations, is subsequently obtained by taking the Fourier transform of $S(q)$. The radial distribution function, $R(r)$, is related to $g(r)$, $R(r)=4\pi r^2\rho_o g(r)$, where ρ_o is the average number density. The utility of $R(r)$ is that an integration over its first peak gives the coordination number. (see Ref. 38) for a full discussion of these points).

Waseda made the first extensive diffraction studies of liquids [39]. The first structural studies of liquids in a containerless environment were neutron diffraction measurements made with EML[40)-42)]. A key observation in the data from those liquids is a peak on the high-q side of the second peak in S(q). Assuming that to lowest order, the liquid structure can be modelled by assuming tightly bound, non-interacting, close-packed, clusters, this split peak is consistent with developing ISRO, arising because the central-to-vertex atomic distance is approximately 5% shorter than the vertex-to-vertex distance. Of course, the assumption of a single cluster to describe the liquid is incorrect. The correct approach to more realistically analyse scattering data from amorphous liquids and glasses is, however, hotly debated. Reverse Monte Carlo (RMC), an inverse Metropolis Monte Carlo method, offers one approach [43)-46)]. The limitations of the RMC method must be recognized, however. It is a maximum entropy approach, producing the most disordered structure that is consistent with the experimental scattering data; it works best for pairwise additive potentials, but not for strongly covalent systems [45)]. Based on our experience in liquid metals, the structures produced by RMC fits are reasonable in terms of characteristic metrics such as bond angle distributions and average dominant atomic local topologies. However, it must be emphasized that chemical information is unreliable, unless the RMC fits are constrained by other experimental data, such as from neutron diffraction or EXAFS studies [45)], or by results from ab-initio MD calculations [47)].

Based on extensive experimental and theoretical studies, it now seems clear that ISRO is a dominant short-range order in transition metal element and transition alloy liquids, and even in some non-transition metal liquids [48)]. Chemical ordering accompanies the topological short-range ordering, with evidence for a chemical ordering transition in some cases [49)]. In addition there are emerging examples of medium-range order (MRO) in liquid (i.e. order extending beyond the nearest-neighbor shell), manifest by a pre-peak in X-ray [47)] and

neutron[50] scattering data. While medium-range order is not uncommon in metallic glasses, that it occurs in the liquid, even above the liquidus temperature, is surprising. Where MRO is observed in binary liquids, the solute and solvent have strong and negative heats of mixing, indicating strong bonding. In such cases, it is likely present even when no pre-peak is observed in the X-ray diffraction data, since observation requires a sufficiently large difference in the form factors of the constituent elements [51].

4.2 Coupling of Liquid Structure with the Nucleation Barrier

Frank's hypothesis linking ISRO to the nucleation barrier was first experimentally demonstrated in a Ti-Zr-Ni liquid [52]. In-situ high-energy X-ray diffraction studies of an electrostatically levitated $Ti_{37}Zr_{42}Ni_{21}$ liquid showed that the first recalescence observed was due to the primary nucleation of an icosahedral quasicrystal (i-phase). The i-phase was not stable at this high temperature [53], and within one to two seconds transformed to the stable C14 Laves phase, producing a second recalescence to a higher temperature. Since the polytetrahedral C14 phase is easy to nucleate [53] and has the larger driving free energy, the preferential nucleation of the i-phase demonstrates that its interfacial free energy with the liquid is less than that of the C14 phase, indicating that it was structurally more similar to the liquid. The S(q) data for the $Ti_{37}Zr_{42}Ni_{21}$ liquid show an increasing prominence of the second shoulder of the second peak, consistent with increasing ISRO; this was subsequently confirmed from RMC fits to the scattering data [54] . It is of interest to note that at the temperature of primary recalescence, the coherence length for the ISRO in the supercooled liquid is approximately 2.1 nm; the estimated critical size for nucleation from CNT at that temperature is approximately 3.5 nm. The comparable values of these estimates suggest that the structure of the liquid plays an important role, acting as a template for the nucleation of the ordered phase.

Since the ISRO in the liquid prevented the nucleation of the stable crystal, it might be imagined that it would favour glass formation. However, as in the case for the Ti-Zr-Ni liquid, it often hinders glass formation, instead leading to the nucleation of a metastable quasicrystal. Whether ISRO helps or hinders glass formation, then, depends partially on the details of the free energy surfaces of all of the accessible phases. However, it is even more complicated. The free energy of the liquid phase and the atomic mobility depend on the structural ordering within the liquid, although how is currently an area of active investigation. When, in addition, the coupled-flux effects of non-stoichiometric primary crystallization are included, it is clear that the role of nucleation in glass formation remains a rich subject warranting further study.

5. Summary and Future Investigations

Nucleation is an area of active interest, for basic as well as practical reasons. The CNT provides a reasonably quantitative description of nucleation processes in liquids for small departures from equilibrium. However, it fails to take into account ordering near the interface with the developing crystal nucleus, which can have a significant influence on nucleation. A simple single order parameter approach was discussed as an illustration of how this might be addressed. However, to more fully account for the influence on crystal nucleation of the chemical and structural ordering that occurs within supercooled liquids will require a multiple order parameter approach, such as outlined by Tanaka [55]. Little of the MD work has focused in a quantitative way on how ordering in the liquid, which impacts all of the parameters important for nucleation, may impact crystallization and hence glass formation. This would seem to be a fruitful direction for future investigation.

Acknowledgement

This work was partially supported by the National Science Foundation under grants DMR–08-56199 and DMR–12-06707 and NASA under grants NNX07AK27G and NNX10AU19G.

References

1) K. F. Kelton and A. L. Greer: Nucleation in Condensed Matter - Applications in Materials and Biology, Elsevier, Amsterdam, 2010.
2) P. F. James: J. Non-Cryst. Solids, **73** (1985) 517.
3) Y. T. Shen, T. H. Kim, A. K. Gangopadhyay and K. F. Kelton: Phys. Rev. Lett., **102** (2009) 4.
4) K. F. Kelton: Solid State Physics, ed. H. Ehrenreich and D. Turnbull, Academic Press, Boston, Vol. **45**, 1991.
5) J. Q. Broughton and G. H. Gilmer: J. Chem. Phys., **84** (1986) 5749.
6) W. J. Ma, J. R. Banavar and J. Koplik: J. Chem. Phys., **97** (1992) 485.
7) U. Gasser, E. R. Weeks, A. Schofield, P. N. Pusey and D. A. Weitz: Sci., **292** (2001) 258.
8) L. Gránásy: Europhysics Lett., **24** (1993) 121.
9) L. Gránásy: J. Non-Cryst. Solids, **162** (1993) 301.
10) L. Gránásy: J. Non-Cryst. Solids, **219** (1997) 49.
11) F. Spaepen: Solid State Physics, ed. H. Ehrenreich and D. Turnbull, Acadmic Press, New York, Vol. **47**, 1994.
12) D. Turnbull, J. Chem. Phys., **20** (1952) 411.
13) C. K. Bagdassarian and D. W. Oxtoby: J. Chem. Phys., **100** (1994) 2139.
14) L. Gránásy and F. Igioi: J. Chem. Phys., **107** (1997) 3634.
15) P. F. Wei, K. F. Kelton and R. Falster: J. Appl. Phys., **88** (2000) 5062.
16) K. F. Kelton: Philos. Trans. R. Soc. Lond. A, Math. Phys. Eng. Sci., **361** (2003) 429.
17) K. F. Kelton: Acta Mater, **48** (2000) 1967.
18) K. C. Russell: Acta Metall, **16** (1968) 761.
19) K. F. Kelton: J. Non-Cryst. Solids, **274** (2000) 147
20) H. Diao, R. Salazar, K. F. Kelton and L. D. Gelb: Acta Mater, **56** (2008) 2585.
21) K. F. Kelton: Philos. Mag. Lett., **77** (1998) 337.
22) B. Vonnegut: J. Coll. Sci., **3** (1948) 563.
23) D. Turnbull: J. Appl. Phys., **20** (1949) 817.
24) D. M. Herlach, R. F. Cochrane, I. Egry, H. J. Fecht and A. L. Greer: Int. Mat. Rev., **38** (1993) 273.

25) W.-K. Rhim, M. Collender, M. T. Hyson, W. T. Simms and D. D. Elleman: Rev. Sci. Instrum, **56** (1985) 307.
26) W.-K. Rhim, S. K. Chung, D. Barber, K. F. Man, G. Gutt, A. J. Rulison and R. E. Spjut: Rev. Sci. Instrum, **64** (1993) 2961.
27) A. J. Rulison, J. L. Watkins and B. Zambrano: Rev. Sci. Instrum, **68** (1997) 2853.
28) T. Meister, H. Werner, G. Lohoeofer, D. M. Herlach and H. Unbehauen: Control Eng. Practice, **11** (2003) 117.
29) N. A. Mauro and K. F. Kelton: Rev. Sci. Instrum, **82** (2011) 035114.
30) A. L. Greer: Acta Metall, **30** (1982) 171.
31) K. F. Kelton and A. L. Greer: J. Non-Cryst. Solids, **79** (1986) 295.
32) K. F. Kelton: J. Alloys Comp., **434** (2007) 115.
33) F. C. Frank: Proc. R. Soc. Lond. A, Math. Phys. Sci., **215** (1952) 43.
34) Y. Q. Cheng, E. Ma and H. W. Sheng: Appl. Phys. Lett., **93** (2008) 111913/1.
35) J. C. Holzer and K. F. Kelton: Acta Metall. Et Materialia, **39** (1991) 1833.
36) D. Holland-Moritz, D. M. Herlach and K. Urban: Phys. Rev. Lett., **71** (1993) 1196.
37) K. Urban, D. Holland-Moritz, D. M. Herlach and B. Grushko: Mat. Sci. Eng., **A178** (1994) 293.
38) T. Egami and S. J. L. Billinge: Underneath the Bragg Peaks - Structural Analysis of Complex Materials, Elsevier, Oxford, 2003.
39) Y. Waseda: The Structure of Non-Crystalline Materials: Liquids and Amorphous Solids, McGraw-Hill International Book Co., New York and London, 1980.
40) D. Holland-Moritz, T. Schenk, R. Bellisent, V. Simonet, K. Funakoshi, J. M. Merino, T. Buslaps and S. Reutzel: J. Non-Cryst. Solids, **312-314** (2002) 47.
41) D. Holland-Moritz, T. Schenk, V. Simonet, R. Bellisent, P. Convert and T. Hansen: J. Alloys Comp., **342** (2002) 77.
42) T. Schenk, D. Holland-Moritz, V. Simonet, R. Bellissent and D. M. Herlach: Phys. Rev. Lett., **89** (2002) 075507.
43) R. L. McGreevy: J. Non-Cryst. Solids, **156-158,** (1993) 949.
44) R. L. McGreevy: Nuc. Instrum. Methods in Phys. Res., A**354** (1995) 1.
45) R. L. McGreevy and J. D. Wicks: J. Non-Cryst. Solids, **192-193** (1995) 23.
46) R. L. McGreevy: J. Phys. Cond. Mat., **13** (2001) R877.
47) N. A. Mauro, V. Wessels, J. C. Bendert, S. Klein, A. K. Gangopadhyay, M. J. Kramer, S. G. Hao, G. E. Rustan, A. Kreyssig, A. I. Goldman and K. F. Kelton, Phys. Rev. B **83** (2011) 184109.
48) N. A. Mauro, J. C. Bendert, A. J. Vogt, J. M. Gewin and K. F. Kelton, J. Chem. Phys. **135** (2011) 044502.
49) V. Wessels, A. K. Gangopadhyay, K. K. Sahu, R. W. Hyers, S. M. Canepari, J. R. Rogers, M. J. Kramer, A. I. Goldman, D. Robinson, J. W. Lee, J. R. Morris and K. F. Kelton: Phys. Rev., B**83** (2011) 094116.
50) D. Holland-Moritz, S. Stueber, H. Hartmann, T. Unruh, T. Hansen and A. Meyer: Phys. Rev., B**79** (2009) 064204.
51) N. A. Mauro and K. F. Kelton: J. Non-Cryst. Solids, **358** (2012) 3057.
52) K. F. Kelton, G. W. Lee, A. K. Gangopadhyay, R. W. Hyers, T. J. Rathz, J. R. Rogers, M. B. Robinson and D. S. Robinson, Phys. Rev. Lett. **90** (2003) 195504/1.
53) K. F. Kelton, A. K. Gangopadhyay, G. W. Lee, L. Hannet, R. W. Hyers, S. Krishnan, M. B. Robinson, J. Rogers and T. J. Rathz: J. Non-Cryst. Solids, **312-314** (2002) 305.
54) T. H. Kim, G. W. Lee, A. K. Gangopadhyay, R. W. Hyers, J. R. Rogers, A. I. Goldman and K. F. Kelton: J. Phys. Cond. Mat., **19** (2007) 452112/1.
55) H. Tanaka: J. Stat. Mech (2010) P12001.

(Received 26 Nov. 2012; Accepted 7 Jan. 2012)